Acta Crystallographica Section F
Structural Biology and Crystallization Communications
ISSN 1744-3091

Comparative crystallization and preliminary X-ray diffraction studies of locked nucleic acid and RNA stems of a tenascin C-binding aptamer

Charlotte Förster,[a]‡ Arnd B. E. Brauer,[a]‡ Svenja Brode,[a] Kathrin S. Schmidt,[a]§ Markus Perbandt,[b] Arne Meyer,[b] Wojciech Rypniewski,[c] Christian Betzel,[b] Jens Kurreck,[a] Jens P. Fürste[a] and Volker A. Erdmann[a]*

[a]Institute of Chemistry and Biochemistry, Free University Berlin, Thielallee 63, 14195 Berlin, Germany, [b]Institute of Biochemistry and Food Chemistry, University of Hamburg, c/o DESY, Notkestrasse 85, Building 22a, 22603 Hamburg, Germany, and [c]Institute of Bioorganic Chemistry, Polish Academy of Sciences, Z. Noskowskiego 12/14, 61-704 Poznan, Poland

‡ These authors contributed equally.
§ Present address: Federal Office of Consumer Protection and Food Safety (BVL), Diedersdorfer Weg 1, 12277 Berlin, Germany.

Correspondence e-mail: erdmann@chemie.fu-berlin.de

Received 27 March 2006
Accepted 30 May 2006

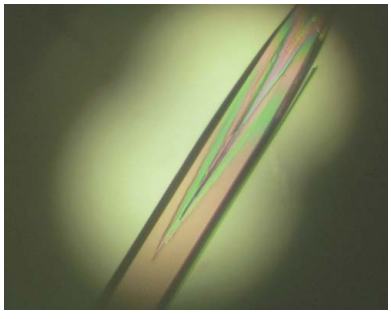

The pharmacokinetic properties of an aptamer against the tumour-marker protein tenascin-C have recently been successfully improved by the introduction of locked nucleic acids (LNAs) into the terminal stem of the aptamer. Since it is believed that this post-SELEX optimization is likely to provide a more general route to enhance the *in vitro* and *in vivo* stability of aptamers, elucidation of the structural basis of this improvement was embarked upon. Here, the crystallographic and X-ray diffraction data of the isolated aptamer stem encompassed in a six-base-pair duplex both with and without the LNA modification are presented. The obtained all-LNA crystals belong to space group $P4_12_12$ or $P4_32_12$, with unit-cell parameters $a = b = 52.80$, $c = 62.83$ Å; the all-RNA crystals belong to space group $R32$, with unit-cell parameters $a = b = 45.21$, $c = 186.97$ Å, $\gamma = 120.00^\circ$.

1. Introduction

Aptamers are nucleic acids that bind specific targets with high affinity and selectivity; they are similar to antibodies in function but are significantly smaller in molecular weight (typically 10–15 kDa; White *et al.*, 2000). They are selected for specific target binding from a large library pool by the SELEX method ('systematic evolution of ligands by exponential enrichment'; Tuerk & Gold, 1990; Ellington & Szostak, 1990). The structural binding properties as well as the therapeutic and analytical potential of aptamers have been reviewed exhaustively (Hermann & Patel, 2000; Nimjee *et al.*, 2005; Tombelli *et al.*, 2005; Rimmele, 2003). Their emerging therapeutic potential is best documented by the US Food and Drug Administration's approval in December 2004 of the first aptamer drug, Macugen, which acts as a selective vascular endothelial growth-factor antagonist in the therapy of neovascular age-related macular degeneration (Gryziewicz, 2005). An example of the diagnostic potential of aptamers is provided by a tenascin-C-binding tumour marker, which has already been used in clinical trials (Hicke *et al.*, 2001, 2006; Schmidt *et al.*, 2004). A stability-enhancing component of this aptamer is the focus of the present communication. The target of this aptamer, tenascin-C, is a large hexameric human glycoprotein found in the extracellular matrix. Following expression during embryogenesis, this protein virtually disappears in the adult organism. However, its expression is sharply up-regulated in tissues undergoing remodelling processes including wound repair, neovascularization, inflammation and tumorigenesis (Hsia & Schwarzbauer, 2005). Based on the latter property, the original tenascin-C-binding aptamer (Hicke *et al.*, 2001) was further developed into a marker for tumour imaging with radioisotopes by several modifications including a 5′-chelator for a technetium-99m label (Schmidt *et al.*, 2004). The proposed secondary structure of the resulting 39-nucleotide aptamer, TTA1, is shown in Fig. 1(*a*). It is presumed to consist of three stem regions which are joined by two loops. Substitution experiments delineate stems II and III as the regions involved in binding, whereas stem I seems to be critical to the stability of the molecule (Hicke *et al.*, 2001). As the molecular integrity is a crucial aspect of the application of aptamers, stem I was modified in order to enhance both the *in vitro* and the *in vivo* stability. The thermal *in vitro* stability, as assessed by the melting

curves of duplexes formed from strand analogues of stem I with the sequence shown in Fig. 1(*b*), was found to follow the order 2′-F/2′-OMe < RNA/RNA ≤ 2′-OMe/2′-OMe < 2′-F/LNA < RNA/LNA = LNA/RNA < 2′-OMe/LNA < LNA/LNA (Schmidt *et al.*, 2004). The highest *in vitro* stability was achieved by the introduction of locked nucleic acids (LNAs), which were first synthesized in the laboratories of T. Imanishi (Obika *et al.*, 1997) and J. Wengel (Singh *et al.*, 1998). The structure of this RNA analogue is depicted in Fig. 1(*c*). LNAs are known to drastically increase the thermal stability and nuclease resistance of oligonucleotides (Kurreck *et al.*, 2002). These improvements are reflected in the altered *in vivo* properties of the correspondingly LNA-modified complete TTA1 aptamer, which include increased nucleolytic stability, slower blood clearance and excretion, improved tumour uptake, and a marginally improved binding affinity (EC_{50} = 2 n*M*; Schmidt *et al.*, 2004). The beneficial effect of the incorporation of LNAs into non-binding stems of aptamers may be a more general way to enhance the *in vitro* as well as the *in vivo* stability of aptamers. In order to obtain structural details of this phenomenon, we have crystallized a six-base-pair duplex encompassing the TTA1 stem I both in the modified LNA/LNA form as well as in the standard RNA/RNA form and collected diffraction data to 1.95 and 2.60 Å resolution, respectively, applying synchrotron radiation.

2. Materials and methods

2.1. Oligonucleotide synthesis and purification

Two LNA oligonucleotides with sequences 5′-ACTCCC-3′ and 5′-GGGAGT-3′ were synthesized on an Applied Biosystems 394 DNA/RNA synthesizer by solid-phase phosphoramidite chemistry with building blocks obtained from Proligo (Hamburg, Germany; in the LNA the building block cytosine is 5-methylated). Oligonucleotides were purified on a Resource 3 ml column (Amersham Biosciences) in the DMT-on mode with a Beckmann HPLC System equipped with a System Gold 168 detector and System Gold 126 solvent modules. Following detritylation, the oligonucleotides were purified again on a Waters XTerra RP18 column (5 µm, 3.9 × 150 mm) using a triethylammonium acetate (TEAA)/acetonitrile (ACN) buffer system (solvent *A*, 50 m*M* TEAA; solvent *B*, 80% ACN in solvent *A*). Two RNA oligonucleotides with sequences 5′-ACUCCC-3′ and 5′-GGGAGU-3′ were synthesized by CureVac GmbH, Tübingen, Germany.

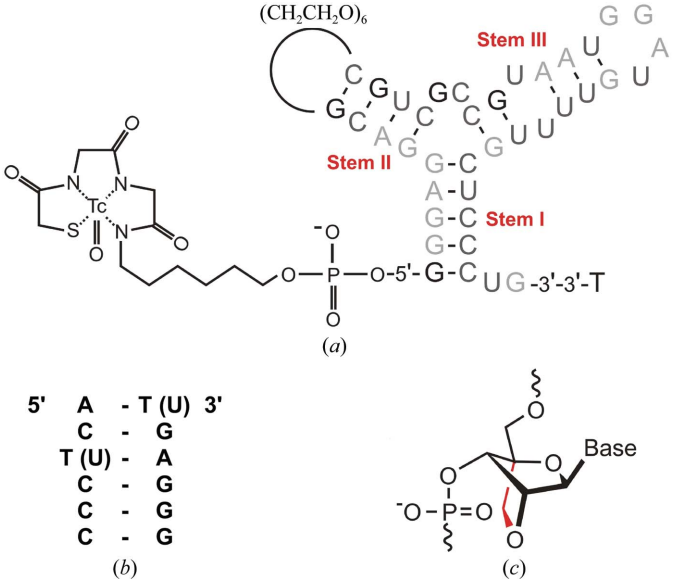

Figure 1
(*a*) Predicted secondary structure of the tenascin-C-binding aptamer with the presumed three helical regions I, II and III (indicated), of which only the latter two are thought to be directly involved in binding. For *in vivo* imaging, the aptamer has been functionalized with 2′-OMe and 2′-F nucleotides (light and dark grey, respectively), a thymidine cap at the 3′-end and a MAG_2 chelate, which is a Cys-Gly-Gly motif conjugated *via* a hexyl-amino linker, at the 5′-end (Hicke *et al.*, 2001; Schmidt *et al.*, 2004). (*b*) LNA (and RNA) sequence of the crystallized stem I following the design described in Schmidt *et al.* (2004). (*c*) Diagram highlighting the additional covalent 2′-*O*,4′-*C*-methylene bridge in the β-D-ribofuranosyl moiety of locked nucleic acids (LNAs).

2.2. Hybridization and crystallization

To obtain the LNA/LNA duplex 5′-ACTCCC-3′/5′-GGGAGT-3′, the two strands, each at a concentration of 0.5 m*M*, were hybridized in water. Analogously, the two strands of the RNA/RNA duplex 5′-ACUCCC-3′/5′-GGGAGU-3′ were hybridized in water at a concentration of 0.5 m*M* each. After heating the respective mixtures to 363 K, they were allowed to cool to room temperature for the formation of duplexes. The resulting solutions were used in subsequent crystallization experiments.

The initial LNA screening was performed with the 48 conditions of the Natrix formulation from Hampton Research (CA, USA), applying the sitting-drop vapour-diffusion technique at 294 K in 96-well CrystalQuick Lp plates (Greiner Bio-One, Germany). A 1 µl sample of 0.5 m*M* LNA/LNA duplex 5′-ACTCCC-3′/5′-GGGAGT-3′ in water was mixed with 1 µl reservoir solution and equilibrated against 80 µl reservoir solution. The crystallization condition with 50 m*M* 2-*N*-morpholinoethanesulfonic acid (MES) pH 5.6, 10 m*M* magnesium chloride and 2.0 *M* lithium sulfate as precipitant was selected as the starting point for an optimization in which the lithium sulfate concentration was varied between 2.0 and 2.25 *M* in increments of 0.05 *M*, applying the hanging-drop vapour-diffusion technique in 24-well Linbro Plates (ICN Biomedicals Inc., Ohio, USA). A 1 µl sample of 0.5 m*M* LNA/LNA duplex in water was mixed with 1 µl reservoir solution and equilibrated against 1 ml reservoir solution at 294 K. 50 m*M* MES pH 5.6, 10 m*M* magnesium chloride and 2.1 *M* lithium sulfate yielded the particularly large crystal used for data collection and shown in Fig. 2(*a*).

The initial RNA screening was also performed with the Natrix formulation applying the sitting-drop vapour-diffusion technique at 294 K in 96-well CrystalQuick Lp plates. A 1 µl sample of 0.5 m*M* RNA/RNA duplex 5′-ACUCCC-3′/5′-GGGAGU-3′ in water was mixed with 1 µl reservoir solution and equilibrated against 80 µl reservoir solution. However, the crystals obtained were very fragile and were not suitable for X-ray diffraction. This included crystals that grew in a comparable time window under the conditions detailed above for the LNA. Much better RNA crystals could be obtained with conditions found by screening with the Nucleic Acid Mini Screen (Hampton Research), applying the hanging-drop vapour-diffusion technique at 294 K in 24-well Linbro Plates; a 1 µl sample of 0.5 m*M* RNA/RNA duplex in water was mixed with 1 µl reservoir solution and equilibrated against 1 ml reservoir solution. A condition consisting of 40 m*M* sodium cacodylate pH 6.0, 12 m*M* spermine–HCl, 80 m*M* sodium chloride and 10%(*v*/*v*) 2-methyl-2,4-pentanediol (MPD) yielded crystals in approximately one week at 294 K which were used for data collection.

2.3. Crystallographic data collection and evaluation

Prior to data collection, LNA crystals were cryoprotected in 50 m*M* MES pH 5.6, 10 m*M* magnesium chloride, 2.1 *M* lithium

Table 1
Data-collection and processing statistics of the all-LNA and all-RNA forms of the TTA1 stem I crystals.

Values in parentheses are for the highest resolution shell.

	LNA	RNA
Beamline	X13 consortium beamline (DESY/HASYLAB)	X13 consortium beamline (DESY/HASYLAB)
Wavelength (Å)	0.80750	0.80630
Space group	$P4_12_12$ or $P4_32_12$	$R32$
Unit-cell parameters (Å, °)	$a = b = 52.80$, $c = 62.83$	$a = b = 45.21$, $c = 186.97$, $\gamma = 120.00$
Matthews coefficient V_M (Å^3 Da^{-1})	2.75	2.45
Measured reflections	119435	16840
Unique reflections	6887	2467
Resolution range (Å)	50–1.95	20–2.60
Completeness (%)	99.3 (100)	99.4 (100)
Multiplicity (%)	17.3 (17.3)	6.8 (7.0)
R_{merge}† (%)	4.5 (40.0)	6.1 (40.1)
Average $I/\sigma(I)$	51.0 (6.8)	22.6 (5.3)

† $R_{merge} = \sum_{hkl}\sum_i |I_i(hkl) - \langle I(hkl)\rangle| / \sum_{hkl}\sum_i I_i(hkl)$, where $I_i(hkl)$ and $\langle I(hkl)\rangle$ are the observed individual and mean intensities of a reflection with indices hkl, respectively, $\sum_i$ is the sum over the individual measurements of a reflection with indices hkl and $\sum_{hkl}$ is the sum over all reflections.

sulfate and 20%(*v*/*v*) glycerol and flash-frozen. RNA crystals were flash-frozen in 40 m*M* sodium cacodylate pH 6.0, 12 m*M* spermine–HCl, 80 m*M* sodium chloride and 10%(*v*/*v*) MPD. X-ray diffraction data were recorded at the X13 consortium beamline (DESY/HASYLAB, Hamburg). For the LNA/LNA duplex, a high-resolution data set from 50 to 1.95 Å was collected at a wavelength of 0.8075 Å. For the RNA/RNA duplex, a data set from 20 to 2.60 Å was collected at a wavelength of 0.8063 Å. Data processing and calculation of the space group and unit-cell parameters were performed with the *HKL*2000 package (Otwinowski & Minor, 1997).

3. Results and discussion

3.1. Crystallization

Fig. 1 shows the predicted secondary structure of TTA1 and the sequence of the crystallized LNA variant of stem I (following the design described in the study of Schmidt *et al.*, 2004). Since LNA is an RNA analogue with an additional covalent 2′-*O*,4′-*C*-methylene cross-link in the ribofuranose moiety designed to 'lock' it in the C3′-*endo* conformation (Fig. 1*c*; Obika *et al.*, 1997; Petersen & Wengel, 2003; Singh *et al.*, 1998), we also crystallized the native RNA counterpart of the TTA1 stem I for a meaningful comparison. We are not aware that a comparison of the crystallization behaviour of LNA compared with RNA duplexes has been reported before and found these to be notably different. In both cases, about 8% of the inital Natrix screen conditions yielded crystals, but only 4% yielded both LNA and RNA crystals. The conditions optimized to obtain LNA crystals (described above; Fig. 2*a*) did not yield RNA crystals that were suitable for X-ray diffraction. RNA crystals thus obtained were very fragile and disintegrated upon handling (Fig. 2*b*). However, with conditions that had been specifically optimized, more robust RNA crystals could be obtained that grew more slowly (Fig. 2*c*). In summary, the optimized LNA crystallization conditions were not equally well suited to crystallization of the corresponding RNA variant. LNA crystals typically appeared overnight and several crystals grew to the size of the crystallization drop. This phenomenon mirrors the gain in stability and rigidity as exemplified by the increase of the melting temperature by increments of approximately 50 K between the RNA and LNA variants (Schmidt *et al.*, 2004).

3.2. Crystallographic data

Table 1 presents a comparison of the crystallographic characteristics of the all-LNA and all-RNA forms of the TTA1 stem I duplex obtained under the individually optimized conditions. While the LNA crystallizes in space group $P4_12_12$ or $P4_32_12$ (corresponding to two molecules per asymmetric unit in the enantiomorph space groups, with a Matthews coefficient V_M of 2.75 Å^3 Da^{-1}), the RNA crystallizes in space group $R32$ (with a Matthews coefficient calculated to be 2.45 Å^3 Da^{-1} considering two molecules per asymmetric unit). A data set was collected to 1.95 Å for the LNA and to 2.60 Å for the RNA. The respective data sets were processed in the resolution ranges 50–1.95 Å with an overall R_{merge} of 4.5% and 20–2.60 Å with an overall R_{merge} of 6.1%. Molecular-replacement calculations are presently in progress using the *CCP*4-associated programs *AMoRe*, *MOLREP* and *Phaser*. A variety of structures are being tested, including a heptameric helix derived from the tRNA^{Ala} acceptor stem (PDB code 434d; Mueller *et al.*, 1999), a dodecameric helix containing the *Escherichia coli* Shine–Dalgarno sequence (PDB code 1sdr; Schindelin *et al.*, 1995) and also an artificial palindromic homodecamer, the sequence of which contains a single LNA

(*a*) (*b*) (*c*)

Figure 2
(*a*) Crystal of the all-LNA form of the TTA1 stem I 6-mer (dimensions of ∼1.4 × 0.2 × 0.2 mm); (*b*) fragile all-RNA crystals grown under the same conditions that were unsuitable for X-ray diffraction; (*c*) RNA crystals suitable for X-ray diffraction obtained under optimized conditions (dimensions typically over 0.5 mm in length and less than 0.05 mm in diameter).

monomer in each strand of DNA (PDB code 1i5w). The latter is to the best of our knowledge the only crystallographic report of LNA in any oligonucleotide setting (Egli *et al.*, 2001). Also important for the analysis, although dissimilar in sequence, are the NMR structures of a nonameric RNA/LNA heteroduplex varying in the balance of LNA to DNA content in the LNA strand (PDB codes 1hhw, 1hhx and 1h0q; Petersen *et al.*, 2002; Nielsen *et al.*, 2004). Partially homologous to the sequence of this study and of particular interest in this context is the recent crystal structure of a decameric all-RNA/all-HNA hybrid, as hexitol nucleic acids (HNAs) also enhance duplex stability by means of conformationally restrained sugar moieties (PDB code 2bj6; Maier *et al.*, 2005).

The structure of the LNA variant of the TTA1 stem I will provide the first crystallographic view of an LNA/LNA duplex. This is a timely investigation because LNAs are now widely used for an ever-increasing number of applications (Jepsen *et al.*, 2004; Jepsen & Wengel, 2004; Kauppinnen *et al.*, 2006; Petersen & Wengel, 2003). Structural investigations in particular have a role in paving the way to a deliberate stability tuning by balancing the properties of RNA and DNA with LNA.

This work was funded in the RiNA Network for RNA Technologies by the Federal Ministry of Education and Research, the City of Berlin and the European Regional Development Fund. We are grateful to Schering AG for making the synthesis facility available and to the Fonds der Chemischen Industrie (Verband der Chemischen Industrie eV) and the National Foundation for Cancer Research, USA for additional support.

References

Egli, M., Minasov, G., Teplova, M., Kumar, R. & Wengel, J. (2001). *J. Chem. Soc., Chem. Commun.*, pp. 651–652.
Ellington, A. D. & Szostak, J. W. (1990). *Nature (London)*, **346**, 818–822.
Gryziewicz, L. (2005). *Adv. Drug Deliv. Rev.* **57**, 2092–2098.
Hermann, T. & Patel, D. J. (2000). *Science*, **287**, 820–825.
Hicke, B. J., Marion, C., Chang, Y. F., Gould, T., Lynott, C. K., Parma, D., Schmidt, P. G. & Warren, S. (2001). *J. Biol. Chem.* **276**, 48644–48654.
Hicke, B. J., Stephens, A. W., Gould, T., Chang, Y. F., Lynott, C. K., Heil, J., Borkowski, S., Hilger, C. S., Cook, G., Warren, S. & Schmidt, P. G. (2006). *J. Nucl. Med.* **47**, 668–678.
Hsia, H. C. & Schwarzbauer, J. E. (2005). *J. Biol. Chem.* **280**, 26641–26644.
Jepsen, J. S., Sorensen, M. D. & Wengel, J. (2004). *Oligonucleotides*, **14**, 130–146.
Jepsen, J. S. & Wengel, J. (2004). *Curr. Opin. Drug Discov. Devel.* **7**, 188–194.
Kauppinnen, S., Vester, B. & Wengel, J. (2006). *RNA Towards Medicine*, edited by V. A. Erdmann, J. Brosius & J. Barciszewski, pp. 405–422. Berlin: Springer.
Kurreck, J., Wyszko, E., Gillen, C. & Erdmann, V. A. (2002). *Nucleic Acids Res.* **30**, 1911–1918.
Maier, T., Przylas, I., Strater, N., Herdewijn, P. & Saenger, W. (2005). *J. Am. Chem. Soc.* **127**, 2937–2943.
Mueller, U., Schübel, H., Sprinzl, M. & Heinemann, U. (1999). *RNA*, **5**, 670–677.
Nielsen, K. E., Rasmussen, J., Kumar, R., Wengel, J., Jacobsen, J. P. & Petersen, M. (2004). *Bioconjug. Chem.* **15**, 449–457.
Nimjee, S. M., Rusconi, C. P. & Sullenger, B. A. (2005). *Annu. Rev. Med.* **56**, 555–583.
Obika, S., Nanbu, D., Hari, Y., Morio, K., Ishida, T. & Imanishi, T. (1997). *Tetrahedron Lett.* **38**, 8735–8738.
Otwinowski, Z. & Minor, W. (1997). *Methods Enzymol.* **276**, 307–326.
Petersen, M., Bondensgaard, K., Wengel, J. & Jacobsen, J. P. (2002). *J. Am. Chem. Soc.* **124**, 5974–5982.
Petersen, M. & Wengel, J. (2003). *Trends Biotechnol.* **21**, 74–81.
Rimmele, M. (2003). *Chembiochem*, **4**, 963–971.
Schindelin, H., Zhang, M., Bald, R., Fürste, J. P., Erdmann, V. A. & Heinemann, U. (1995). *J. Mol. Biol.* **249**, 595–603.
Schmidt, K. S., Borkowski, S., Kurreck, J., Stephens, A. W., Bald, R., Hecht, M., Friebe, M., Dinkelborg, L. & Erdmann, V. A. (2004). *Nucleic Acids Res.* **32**, 5757–5765.
Singh, S. K., Nielsen, P., Koshkin, A. K., Olsen, C. E. & Wengel, J. (1998). *J. Chem. Soc., Chem. Commun.*, pp. 455–456.
Tombelli, S., Minunni, M. & Mascini, M. (2005). *Biosens. Bioelectron.* **20**, 2424–2434.
Tuerk, C. & Gold, L. (1990). *Science*, **249**, 505–510.
White, R. R., Sullenger, B. A. & Rusconi, C. P. (2000). *J. Clin. Invest.* **106**, 929–934.